Abbreviated title: White matter development predicts visual responses

Development of the visual white matter pathways mediates development of electrophysiological responses in visual cortex

Sendy Caffarra[a,b,c*], Sung Jun Joo[d], David Bloom[e,f], John Kruper[e,f], Ariel Rokem[e,f] and Jason D. Yeatman[a,b]

caffarra@stanford.edu, sungjun@pusan.ac.kr, bloomdt@gmail.com, jk232@uw.edu, arokem@gmail.com, jyeatman@stanford.edu

[a] Stanford University School of Medicine, Division of Developmental-Behavioral Pediatrics, Stanford, CA 94305, USA.

[b] Stanford University Graduate School of Education, Stanford, CA 94305, USA.

[c] Basque Center on Cognition, Brain and Language, San Sebastian 20009, Spain.

[d] Department of Psychology, Pusan National University, Pusan 46241, Republic of Korea.

[e] Department of Psychology, University of Washington, Seattle, WA 91905, USA.

[f] eScience Institute, University of Washington, Seattle, WA 98195-1570, USA.

*Corresponding author:

Sendy Caffarra, Center for Education Research at Stanford (CERAS)

520 Galvez Mall, Stanford, CA 94305, http://orcid.org/0000-0003-3667-5061

Conflict of interest disclosure: The authors declare no competing financial interests.

Funding statement: This project has received funding from the European Union's Horizon 2020 research and innovation programme under the Marie Sklodowska-Curie grant agreement No 837228 to SC, and was supported by the National Research Foundation of Korea (NRF) grant funded by the Korea government (MSIT) (No. NRF-2019R1C1C1009383) to SJJ. This work was also supported by NSF/BSF BCS #1551330, NICHD R01HD09586101, NICHD R21HD092771 and Jacobs Foundation Research Fellowship to JDY and RF1MH121868-01 to AR and JDY

Data availability statement: Code and data to reproduce the reported findings are available at [INSERT URL UPON PUBLICATION]

Ethics approval statement: The study was approved by the Institutional Review Board.

Abstract

The latency of neural responses in the visual cortex changes systematically across the lifespan. Here we test the hypothesis that development of visual white matter pathways mediates maturational changes in conduction velocities of visual signals. Thirty-eight children participated in a cross-sectional study including diffusion MRI and MEG sessions. During the MEG acquisition, participants performed a lexical decision and a fixation task on words presented at varying levels of contrast and noise. For all stimuli and tasks, early evoked fields were observed around 100 ms after stimulus onset (M100), with slower and lower amplitude responses for low as compared to high contrast stimuli. The optic radiations and optic tracts were identified in each individual's brain based on diffusion MRI tractography. The diffusion properties of the optic radiations predicted M100 responses, especially for high contrast stimuli. Higher optic radiation fractional anisotropy (FA) values were associated with faster and larger M100 responses. Over this developmental window, the M100 responses to high contrast stimuli became faster with age and the optic radiation FA fully mediated this effect. These findings suggest that the maturation of the optic radiations over childhood accounts for individual variations observed in the developmental trajectory of visual cortex responses.

Keywords: tractography, MEG, visual system, childhood, diffusion MRI

Introduction

Electrophysiological responses in visual cortex are subject to a high degree of variability. It is known that these responses reliably differ among individuals and change over development (Allison et al. 1984; Onofrj et al. 2001). Being able to account for these variations will improve our understanding of the brain circuits and their developmental trajectories in health and disease. One possible source of variability in electrophysiology lies in structural properties of the white matter tracts (Kanai and Rees 2011; Wandell 2016), which carry signals to the cortex. In the last two decades, novel neuroscientific tools (including tractography) have opened the possibility to address this question and explore the relation between functional and structural properties of the brain (Jeurissen et al. 2019; Wandell 2016). In this study we combine diffusion magnetic resonance imaging (dMRI) and tractography with magnetoencephalography (MEG), to examine the variability of visual responses during childhood. We asked whether developmental differences in visual response properties are the result of the maturation of the white matter pathways carrying visual signals. Specifically, we test the hypothesis that developmental variations of visual pathways mediate age effects on electrophysiological responses.

In neurologically healthy individuals, any visual input elicits electrophysiological responses roughly 100 ms after stimulus presentation, though the precise timing varies by as much as 50 ms among individuals (Allison et al. 1984; Kolb, Fernandez, and Nelson 2005; Odom et al. 2004; Spear 1993; Vialatte et al. 2010). These visually evoked responses can be recorded over the occipital part of the scalp and have their neural source in the early visual cortex. There is consistent evidence that the latency of visual responses change substantially across the lifespan, with a speed increase of 10 ms per decade within the first 20 years of age and a symmetrical slow down after 60 years of age (Armstrong, Slaven, and Harding 1991; Allison et al. 1984; Onofrj et al. 2001; Spear 1993). The nature of these latency changes is still poorly understood, but clinical research suggests that the structural properties of visual white matter pathways can play a crucial role in determining the conduction velocity of visual signals. Studies on patients with demyelinating lesions of the visual tracts have shown that white matter diffusion properties (such as fractional anisotropy, FA, or mean diffusivity, MD) predict delays in the electrophysiological responses of the visual cortex (Alshowaeir et al. 2014; Berman et al. 2020; Kolbe et al. 2012; Lobsien et al. 2014; Naismith et al. 2010; M. Y. Takemura et al. 2017). For instance, patients with lower FA or higher MD of the optic radiations (the tract connecting the lateral geniculate nucleus

to the primary visual cortex; Figure 1) showed slower visually evoked responses. These results suggest that the demyelination of visual pathways (reflected by altered diffusion properties) accounts for conduction delays of visual signals that are carried from the eyes to the visual cortex, and ultimately explains the latency variability of evoked responses recorded on the scalp in patient populations.

The relation between visual white matter properties and electrophysiology has recently been reported in one study of healthy adults (H. Takemura, Yuasa, and Amano 2020). This suggests that there may be sufficient variability in the organization of the optic radiations among typical adults that the structural differences affect signaling properties in the visual system. Moreover, two additional studies have reported a similar structural-functional relationship in the infant (1-4 months, Dubois et al. 2008) and in the ageing brain (18-88 years, Price et al. 2017). Despite these new research findings, the amount of evidence showing links between electrophysiological responses and white matter properties is still scarce, and mainly related to clinical populations. In addition, the age range from 1 to 18 years old remains fully unexplored.

Childhood represents a crucial developmental phase where many visual circuits reach maturity (Allison et al. 1984; Gilmore, Knickmeyer, and Gao 2018; Onofrj et al. 2001; Siu and Murphy 2018). Moreover, this is a developmental window where white

matter pathways are still rapidly changing and approaching maturity (Lebel et al. 2008, 2012; Yeatman, Wandell, and Mezer 2014). However, the potential relationship between these structural and functional maturational variations is yet to be described. The present study links the structural and functional properties of the visual system in childhood by combining dMRI with MEG. We show that the maturational differences of the optic radiations observed during childhood fully mediate age effects on visually evoked responses.

Materials and Methods

Participants

Forty-six children participated in a cross-sectional study including a dMRI and an MEG session. All the data were manually inspected for quality of the MEG recordings and artifacts in the dMRI data, and 8 participants were excluded leaving a final sample size of thirty-eight (17 females, mean age: 9.5 y, SD: 1.6, age range: 7-12 y, between-sessions time gap: 0-35 dd). All participants had normal or corrected-to-normal vision, and no history of neurological, psychiatric, or sensory disorder. All parents (or legal guardians) signed a written informed consent, and all participants gave their verbal assent. The study was conducted in accordance with the guidelines of

the University of Washington Subjects Division and was approved by the Institutional Review Board.

Based on the average of the correlations reported in a previous study of healthy adults using a similar methodology (r_{avg}=0.48; H. Takemura, Yuasa, and Amano 2020), the present sample size ensures a statistical power of at least 0.87 (Hulley et al. 2001).

MEG materials and experimental design

The MEG data analyzed here came from a previous study on automaticity in the brain's reading circuitry (Joo et al. 2021). In the present study we focused on the earliest MEG responses evoked by the visual stimuli. Visual words were presented at two contrast levels (high and low: HC and LC) and two noise levels (high and low: HN and LN). Two hundred and forty images of four-letter English words were rendered in Courier font. Visual stimuli had a Weber contrast of 7.8% or 100%. In addition, each visual stimulus was mixed with a different percentage of noise (20% or 80%), corresponding to the phase-scrambled version of the original image. This procedure led to the creation of readable (20% of noise, LN) and unreadable experimental stimuli (80% of noise, HN).

The images were presented in four separate runs and repeated twice (eight runs in total). Two different tasks were carried out in alternating runs on the identical set of stimuli: a fixation task and a lexical decision task. In order to make these tasks possible,

a colored fixation dot was added at the center of the screen and a small set of pseudowords (n=11) was presented for each run together with the rest of the experimental stimuli. In the fixation task, participants had to press a response button when a fixation dot turned red. In the lexical decision task, participants had to press a response button when a pseudoword was presented.

During each MEG experimental trial, a visual stimulus appeared on the screen for 1 sec and was followed by a blank with a random duration between 620 and 840 ms (see Figure 1). A colored fixation dot was always present in the center of the screen and changed its color every 500 ms (among the following options: green, blue, yellow, cyan or red). The stimuli were presented on a gray background (50 cd/m^2) and subtended 2.7 degrees at a viewing distance of 1.25 m.

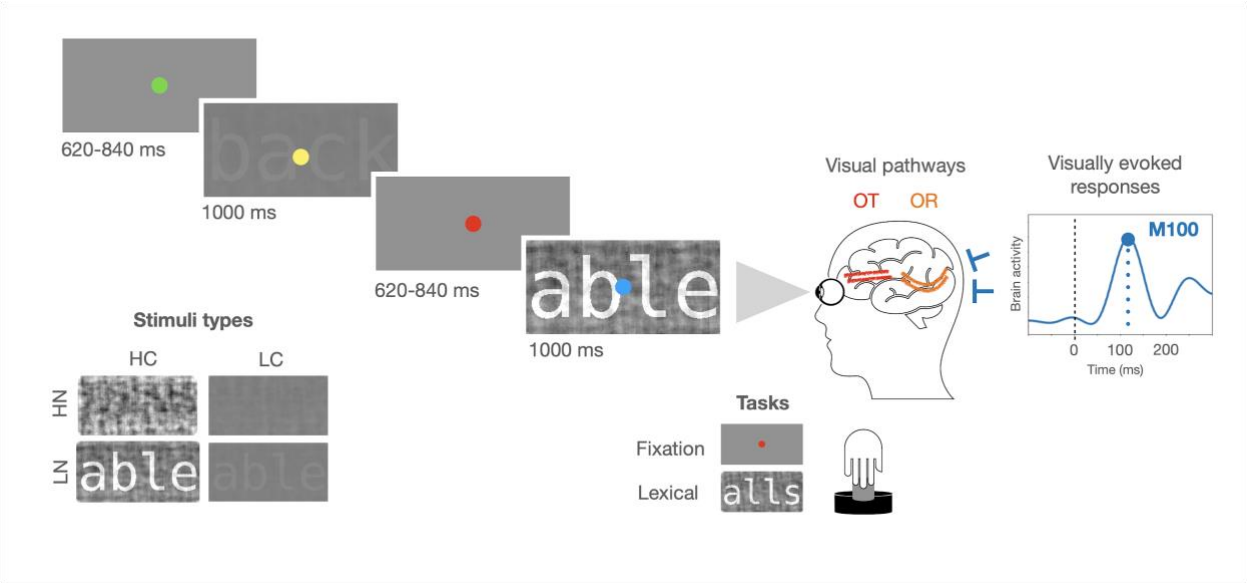

Figure 1. Schematic representation of an MEG experimental trial, the experimental conditions, and the visual pathways. Stimuli could show at a high or low level of contrast (HC or LC), and at a high or low degree of noise (HN or LN). The task required

a button press whenever the fixation dot turned red (fixation task) or whenever a pseudoword was presented (lexical decision task). Visual information is received by the eyes and carried through the visual pathways (including the optic nerve, the optic tract (OT) and the optic radiation (OR)) to the visual cortex, where visually evoked responses can be recorded through MEG sensors. A magnetic evoked response peaking around 100 ms (M100 response, dotted line) from a subject of the present study (S172: male, 9 years old) is displayed here as a representative example of visually evoked response.

MEG acquisition and pre-processing

MEG data were recorded in a magnetically shielded room (Maxshieldł, Elekta Oy, Helsinki, Finland) using an Elekta-Neuromag MEG device (including 102 sensors with two planar gradiometers and one magnetometer each). MEG recordings were acquired continuously with children in sitting position, with a bandpass filter at 0.01−600 Hz and a sampling rate of 1.2 KHz. Head position inside the helmet was continuously monitored using head position indicator coils. The location of each coil relative to the anatomical fiducials (nasion, and left and right preauricular points) was defined with a 3D digitizer (Polhemus Fastrak, Colchester, VT, USA). About 100 head surface points were digitized.

MEG data were analyzed using MNE-Python (Gramfort et al. 2013). The signal was subjected to noise reduction using the Maxwell filter function and data were individually corrected for head movements using the average of participants' initial head positions as a reference. The temporally extended signal space separation method was applied with a correlation limit of 0.98 and a segment length of 10 sec (Taulu and Hari 2009; Taulu and Kajola 2005). Bad channels were substituted with interpolated

values. An Independent Component Analysis (ICA) was applied to the down-sampled and filtered MEG continuous signal (each 5th data point was selected, Gramfort et al. 2013). Downsampling was only used for the ICA analysis and it was not applied in the subsequent preprocessing steps. Independent components corresponding to the heartbeat and ocular artifacts were automatically identified and removed from the filtered MEG signal based on cross-trial phase statistics with the ECG and EOG channels (Dammers et al. 2008). The average number of rejected components was 3 (SD: 1.7). MEG epochs were obtained, including 0.6 sec before and 1.6 second after the visual presentation onset. Residual artifacts exceeding a peak-to-peak amplitude of 1000e-12 fT/cm for gradiometers and of 4000e-14 fT for magnetometers were automatically rejected. On average, 6% (SD: 8.4) of trials were rejected, with no significant difference across conditions ($F(7,296)=0.09$, $p=0.99$).

To obtain evoked related fields (ERF), artifact-free trials were low-pass filtered (firwin method was used with upper passband edge of 40 Hz, filter length: 331 ms), averaged and baseline corrected (-0.6-0 s). ERFs were calculated for each condition and each participant and they were quantified by computing the root mean square of the two gradiometers in each pair.

For each main effect (contrast, noise, and task), ERFs were statistically compared using a nonparametric cluster-based permutation test (Maris and Oostenveld 2007). Specifically, *t*-statistics were computed for each sensor and time point during the 0 – 800

ms time window, and a clustering algorithm formed groups of channels over time points based on these tests. In order for a data point to become part of a cluster, a threshold of $p = 0.05$ was used (based on a two-tailed dependent t-test, using probability correction). The sum of the t-statistics in a sensor group was then used as a cluster-level statistic, which was then tested with a randomization test using 1000 runs.

The M100 peak was identified for each participant as the highest amplitude fluctuation within the spatio-temporal cluster previously identified by the cluster-based permutation (occipital sensors, 80-150 ms; see Figure 2). The M100 latency was estimated as the time point at which the M100 amplitude reached 50% of the peak value (this relative criterion represents one of the most accurate methods to estimate the latency of evoked responses and it ensures higher statistical power compared to absolute criteria, Kiesel et al. 2008). The corresponding M100 amplitude value was also extracted for each participant.

Any significant ERF effect was reconstructed in the source space. A cortical MEG source space was constructed using dipoles with 3 mm spacing. These were constrained to be normal to the cortical surface using Freesurfer (Dale, Fischl, and Sereno 1999). A forward solution was calculated to map dipole currents in the source space to the sensor space (Mosher et al. 1999). Dipole currents in this whole-brain source space were estimated from the evoked MEG response. A minimum-norm linear estimation (MNE) approach was employed (Dale, Fischl, and Sereno 1999; Hämäläinen and Ilmoniemi

1994; Hämäläinen and Sarvas 1989) with sensor noise covariance estimated from 100 ms epochs prior to each trial onset. Source localization data were then mapped to an average brain (freesurfer averaged brain) using a non-linear spherical morphing procedure (20 smoothing steps) that optimally aligns individual sulcal–gyral patterns (Fischl et al. 1999).

To more completely describe the electrophysiological properties of visually evoked responses, we characterized the M100 response within the time-frequency domain. This method explores single MEG trials within a narrow frequency band. By doing this, the amplitude of the noise is considerably reduced as compared to single-trial evoked responses (Herrmann et al. 2014). Also, the interpretation of time-frequency properties can be better related to the degree of synchronization of neural oscillatory activity (Zhang 2019).

Time-frequency representations (TFR) of power and inter-trial coherence values were calculated using Morlet wavelets on the unfiltered data. Single-trial time-frequency values were decomposed between 1 and 20 Hz (in steps of 1Hz), with a width of the wavelets equal to the half of the frequency under interest. The resulting values were averaged across trials for each condition and each participant. Our visually evoked responses were evident also in the time-frequency domain as the most prominent power and inter-trial coherence modulation over occipital sensors around 100 ms after stimulus presentation (see Figure 2). Maximum values of M100 power and

inter-trial coherence were extracted for each subject using a similar spatio-temporal cluster employed for the ERFs values extraction (occipital sensors, 0-200 ms, 1-8 Hz; this was the result of a cluster-based permutation analogous to the one performed for the ERFs).

Diffusion MRI acquisition and pre-processing

Imaging data were recorded using a 3 T Phillips Achieva scanner (Philips, Eindhoven, Netherlands) at the University of Washington Diagnostic Imaging Sciences Center with a 32-channel head coil. Head motion was minimized by an inflated cap, and participants were monitored through a closed-circuit camera system. Diffusion-weighted magnetic resonance imaging (dMRI) data were acquired with a spatial resolution of 2.0 mm^3 and full brain coverage. A diffusion-weighted imaging (DWI) scan was acquired with 64 non-collinear directions (b-value = 2000 s/mm^2) with a TR of 7700 ms and a TE of 85 ms. The DWI scan also contained 4 volumes without diffusion weighting (b-value = 0). In addition, one scan with six non-diffusion-weighted volumes with a reversed phase encoding direction (posterior-anterior) was collected to correct for echo-planar imaging distortions related to inhomogeneities in the magnetic field.

The T1-weighted (T1w) images were corrected for intensity non-uniformity (INU) using N4BiasFieldCorrection (Tustison et al. 2010, ANTs 2.3.1), and used as T1w-reference throughout the workflow. The T1w-reference was then skull-stripped using

antsBrainExtraction.sh (ANTs 2.3.1), using OASIS as target template. Spatial normalization to the ICBM 152 Nonlinear Asymmetrical template version 2009c (Fonov et al. 2009) was performed through nonlinear registration with antsRegistration (ANTs 2.3.1, Avants et al. 2008), using brain-extracted versions of both T1w volume and template. Brain tissue segmentation of cerebrospinal fluid (CSF), white-matter (WM) and gray-matter (GM) was performed on the brain-extracted T1w using FAST (FSL 6.0.3, Zhang, Brady, and Smith 2001).

Preprocessing and reconstruction were carried out using QSIprep 0.11.5 (https://qsiprep.readthedocs.io/, based on Nipype 1.5.0; (Cieslak et al. 2020; Gorgolewski et al. 2011; Gorgolewski et al. 2018), which included topup distortion, motion and eddy current correction (Andersson and Sotiropoulos 2016; Andersson, Skare, and Ashburner 2003; Smith et al. 2004). Multi-tissue fiber response functions were estimated using the dhollander algorithm as implemented in MRtrix3 (Tournier et al. 2019). Fiber orientation distributions (FODs) in each voxel were estimated via constrained spherical deconvolution (CSD, Tournier et al. 2004, 2008) using an unsupervised multi-tissue method (Dhollander et al. 2019; Dhollander, Raffelt, and Connelly 2016). FODs were intensity-normalized using mtnormalize (Raffelt et al. 2017). Probabilistic tractography was carried out using the default parameters implemented in QSIprep (10M streamlines, minimum length: 30 mm, maximum length: 250 mm). The left and the right optic radiations were identified using vistasoft

(https://github.com/vistalab/vistasoft) based on two endpoint regions of interest (ROIs) corresponding to the primary visual cortex and the central part of the thalamus including the lateral geniculate nucleus (defined based on the AICHA atlas, Joliot et al. 2015); minimum distance 3 mm). To further clean the tract from crossing fibers (Fan et al. 2016; Sherbondy et al. 2008), three exclusion ROIs were also used (temporal pole, and occipital pole from the AICHA atlas, and the posterior portion of the thalamus based on the brainnetome atlas; (Fan et al. 2016; Sherbondy et al. 2008). All ROIs were defined in a MNI template and transformed to each participant's native space using QSIprep. A final cleaning step was carried out to remove outlier fibers based on streamline average length and mean Gaussian distance from the bundle core (threshold of 3 SD; Yeatman et al. 2012). The optic radiations were clipped at the endpoint ROIs (minimum distance: 3 mm) to avoid potential partial volume effects at the white matter/gray matter border (see Figure S1 in the Supplementary Materials for a schematic representation of the bundle segmentation pipeline). The diffusion data was then fitted with the tensor model using a standard least-squares algorithm. Diffusion metrics were projected onto the previously identified optic radiations and fractional anisotropy (FA) was mapped onto each tract. The average FA value of the two optic radiations was calculated for each participant.

A similar approach was taken to identify the optic tract. A first endpoint ROI corresponded to the central part of the thalamus used for the optic radiations

(minimum distance 3 mm). A second waypoint ROI (minimum distance 3 mm) was manually defined at the center of the optic chiasm of each participant (5 mm sphere; mean coordinates of the center: 0, +3, -16). The tract was further cleaned by removing outlier fibers based on streamline average length and mean distance from the bundle core (threshold of 2 and 3 SD, respectively). The average FA value of the two OTs was calculated for each participant.

Two additional white matter tracts that were not part of the visual system (left uncinate and left corticospinal tract) were segmented and average FA values were calculated using pyAFQ (https://yeatmanlab.github.io/pyAFQ; (Yeatman et al. 2012; Kruper et al. 2021). These tracts were used as control pathways as they are not supposed to carry visual signals.

Statistical analysis

To test the relationship between structural properties of the optic radiations and speed of visual responses, a Pearson correlation between mean FA values and M100 latency was calculated. To make sure that the FA effect on electrophysiology held after accounting for developmental differences, M100 latency was also analyzed using a linear regression model including FA and Age as predictors. The effect of age on electrophysiological responses was further examined using a causal mediation analysis as implemented in (Tingley et al. 2014). After checking for an age effect on M100 latency

and optic radiations FA values, we tested whether optic radiations FA values mediated M100 developmental variations. Statistical analyses were carried out with R 4.0.0 (https://www.R-project.org/) using the mediation package (Tingley et al. 2014).

Secondary analyses concerned the other properties of the M100 response. Similar FA-M100 correlations, regressions and mediation analyses were carried out with additional electrophysiological properties of the M100 response (M100 peak amplitude, power, and inter-trial coherence) to further understand the relation between structural and functional properties of the visual brain network.

Results

Behavioral results

Participants paid attention to the visual stimuli, as shown by the intermediate-to-high levels of accuracy in the fixation task (median accuracy: 81% correct, IQR: 35; median RT: 547 ms, IQR: 124). The lexical task showed lower accuracy and slower responses as a result of children's variable reading skills (median: 17%, IQR: 15; median RT: 880 ms, IQR: 391). No significant correlation was observed between these behavioral performances and the structural or functional brain measures described below (all *p*s>.05).

MEG results

The M100 responses showed substantial modulations based on the contrast of the image (see Figure 2) and did not change based on image noise or cognitive task. In accordance with previous electrophysiological studies (Abdullah et al. 2012; Gebodh, Vanegas, and Kelly 2017; Maddess, James, and Bowman 2005), high contrast stimuli elicited larger and faster M100 responses as compared to low contrast stimuli (p<.001). The response was 8 ms faster and 57% larger for high contrast compared to low contrast stimuli. No other main effects (noise or task) or interactions could be observed in the M100 response (ps>.05).

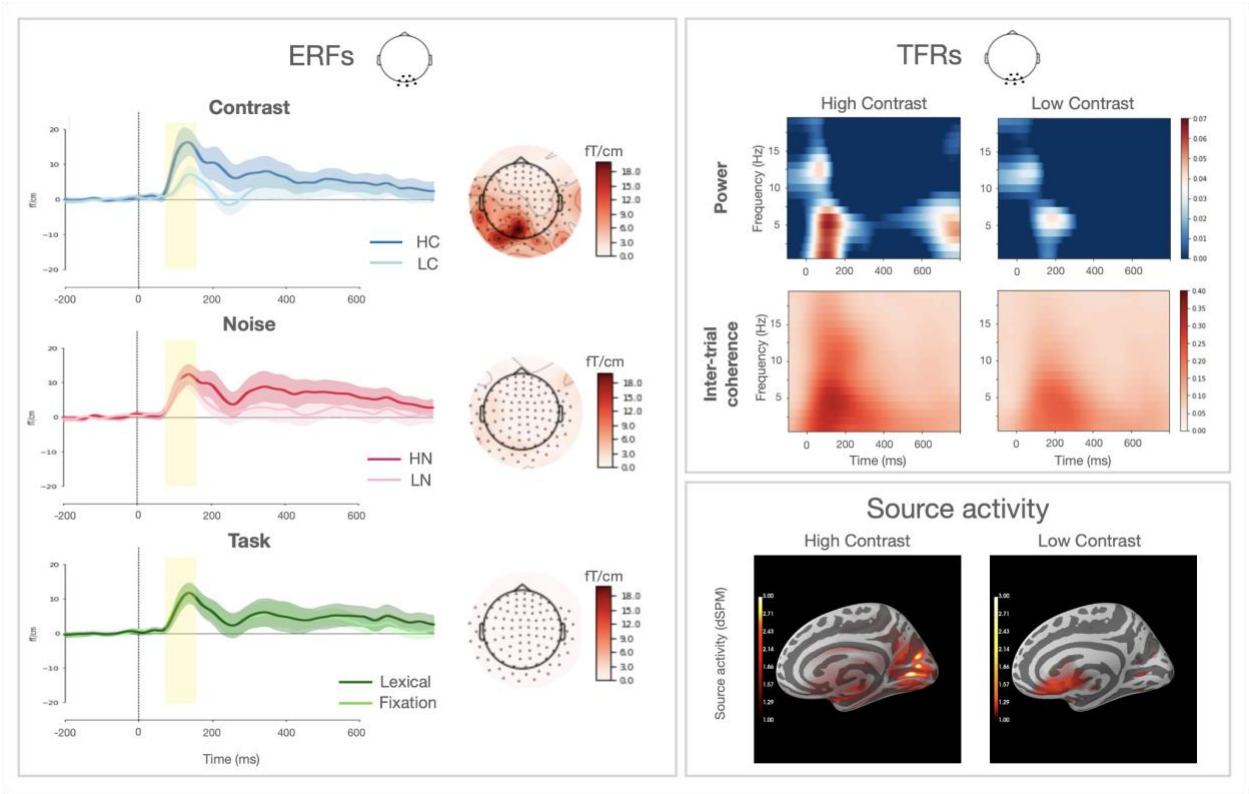

Figure 2. ERFs panel: ERF responses to different levels of contrast, noise, and task over an occipital cluster of sensors. The yellow box represents the time window where the

main effect of contrast reached its maximum (80-150 ms). Topographic distribution of each effect at 100 ms (calculated as the difference within each condition pair) is displayed on the right side. **TFRs panel:** TFR of power and inter-trial coherence for occipital sensors. Only HC and LC conditions are represented here. Power values are expressed as the relative change (logratio) from a baseline interval between -0.4 and -0.2 ms. **Source Activity panel:** the neural source of the M100 response is represented for the HC and LC conditions.

Linking MEG responses to visual white matter pathways

Given that high contrast stimuli elicited sharper and more reliable evoked responses in the visual cortex, we report here the correlation and mediation results relative to this condition (for the low contrast stimuli, see Figure S2 in the Supplementary Materials). M100 latency correlated with individual optic radiations FA values (r=-0.35, p=0.02; robust r=-0.32, p=0.03); children with higher FA had faster M100 responses than children with low FA (see Figure 3). This effect remained significant after accounting for age (β=-338, SE=193, $t(35)$=1.8, p=0.04). The relationship with electrophysiology was specific to this visual pathway as it was not observed for white matter tracts that do not carry visual information (e.g., left uncinate: r=-0.06, p=0.35; left corticospinal tract: r=-0.10, p=0.28).

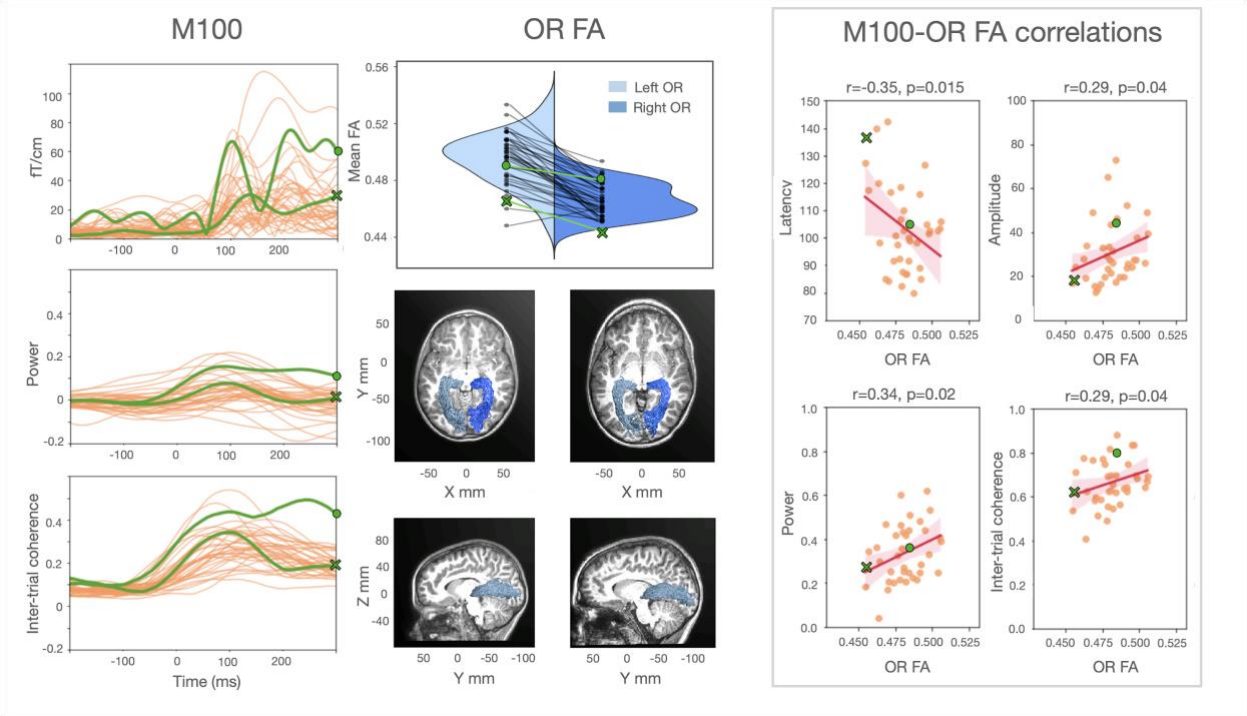

Figure 3. The relation between structural and functional properties of the visual pathways. **M100 panel:** Individual waveforms to high contrast stimuli from a central occipital sensor pair. ERFs, power and inter-trial coherence average values (between 1 and 8 Hz) are displayed over time. The occipital responses of two representative subjects (S210: female, 7 years old; and S227: male, 11 years old) are marked in green to highlight individual differences. The dot and the cross green markers correspond to the faster and the slower individual, respectively. **OR FA panel:** Violin plot of the individual FA values from the left and right optic radiations. Green markers correspond to the FA values of the same two representative subjects. Sagittal and axial views of the optic radiations for the two representative participants are overlaid on each subject's structural image. **M100-OR FA correlations panel:** Correlations between MEG measures and optic radiations FA mean values. Data points of the two representative participants are marked with a green dot and a green cross. Similar, although weaker, findings were found for low contrast stimuli (see Figure S2 in the Supplementary Materials).

M100 responses and FA values for the optic radiations showed age effects between ages 7 and 12. With greater age, M100 responses were faster (r=-0.31, p=0.03) and FA values were higher (r=+0.30, p=0.03, see Figure 4). Optic radiations FA values

mediated the effect of age on electrophysiological responses (average causal mediation effect: β=-0.07, *CI* [-0.20; -2.0e-3], p=0.04; mediated percentage estimate: 28%, p=0.02). The effect of age on M100 latency was not significant after adding FA as a mediator (average direct effect: β=-0.19, *CI* [-0.42; +0.08], p=0.14), indicating that maturational variations of optic radiations FA fully mediated age effects on M100 latency.

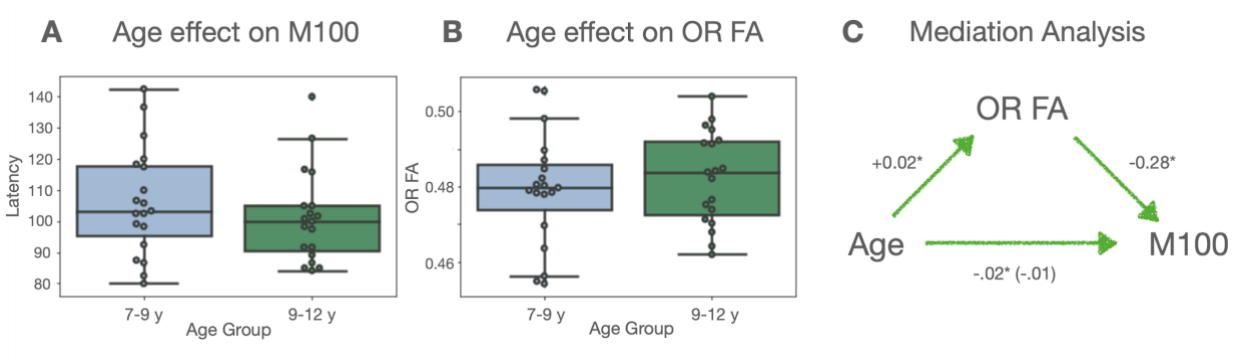

Figure 4. A and B: Age differences in M100 latency and optic radiations FA values (age groups were defined based on a median split; younger group: 7-9 years; older group: 9-12 years). **C:** the results of the causal mediation analysis are summarized.

Similar FA correlations were found with the other M100 electrophysiological properties (amplitude: r=+0.29, p=0.04, robust r=+0.35, p=0.02; power: r=+0.34, p=0.02, robust r=+0.34, p=0.02; inter-trial coherence: r=+0.29, p=0.04, robust r=+0.29, p=0.04). Children with high values of optic radiations FA showed higher M100 amplitude, power and inter-trial coherence (see Figure 3 and 4). After correcting for age, the FA effects on M100 amplitude and power remained significant (amplitude: β=3.1e-11, *SE*=1.8e-11, $t(35)$=1.8, p=0.04; power: β=3.0, *SE*=1.6, $t(35)$=1.9, p=0.03; inter-trial coherence: β=1.7, *SE*=1.3, $t(35)$=1.3, p=0.2). Finally, FA mediation effects were confirmed for M100

amplitude and power (amplitude: β=6.5e-15, *CI* [+4.2e-17; +1.8e-14], p=0.04; power: β=6.3e-4, *CI* [+2.4e-5, +1.6e-3], p=0.04; inter-trial coherence: β=3.6e-4, *CI* [-7.4e-5; +1.1e-3], p=0.13).

Does maturation of the optic tract account for additional variance in electrophysiology?

We next ask whether other stages of the visual pathway additively predict variance in visual responses. The correlation between M100 latency and optic tract FA was not significant, although the direction was similar to the optic radiations correlation (r=-0.20, p=0.12). Adding the optic tract FA to a regression model including the optic radiations FA did not improve the model fit to the M100 latencies ($\chi^2(1)$=0.13, p=.72). Similar results were obtained with the other electrophysiological features (amplitude: r=-0.14, p=0.20, $\chi^2(1)$=3.31, p=.08; power: r=+0.14, p=0.19, $\chi^2(1)$=5e-4, p=.98; inter-trial coherence: r=+0.15, p=0.19, $\chi^2(1)$=0.04, p=.85). Moreover, we did not find a significant correlation between optic tract FA and age (r=+.11, p=.25). These findings suggest that FA values in the optic tract are largely stable by late childhood and that individual differences in the optic tracts do not account for additional variance in M100 responses.

Task and stimulus effects

To examine whether the relationship between M100 responses and optic radiations diffusion properties changed as a function of the stimulus or task, we compared different linear mixed effects (LME) models where M100 latency was the dependent variable. We started with a simple model with by-subject random intercepts, including the factors Image Contrast, optic radiations FA, and their interaction. We found a significant main effect of image contrast indicating that low contrast images produce later M100 responses than high contrast images (β=5.29, *SE*=0.95, *t(265)*=5.54, p<.001), and a significant FA by contrast interaction indicating that FA only predicted M100 latency for high contrast images (β=121.12, *SE*=70.82, *t(264)*=1.71, p=.04). We progressively added the factors Task, Noise, and their interactions with the other factors. None of these more complex models improved the original model fit (all χ^2<14, all *ps*>.10) and none of the fixed effects reached significance (all ps>.06). This was true also for M100 amplitude (all χ^2<12, all *ps*>.19) and power (all χ^2<12, all *ps*>.17). In the models on inter-trial coherence adding the factor Noise and its interactions slightly improved the model fit (all $\chi^2(8)$=36.6, all *p*<.001), but follow-up analyses just confirmed the main effect of the optic radiations FA (β=2.26, *SE*=1.01, *t(36)*=2.25, *p*=.03). These results suggest that the link between structural and functional properties of the visual pathways observed here can be generalized to different types of visual stimuli (e.g.,

words vs. noise patches) and different cognitive tasks (e.g., color judgment and lexical decision).

Discussion

This study describes the link between structural and functional properties of children's visual pathways and how they change during childhood. We combined dMRI and MEG to measure properties of children's visual white matter tracts (optic radiations and optic tracts), as well as electrophysiological properties of their visually evoked responses (M100 responses). The data showed that: (1) the structural properties of the optic radiations (indexed by FA values) vary among children and part of this variability is accounted for by age; (2) the electrophysiological properties of the responses in the visual cortex are highly variable in childhood and part of this variability is also explained by age; (3) there is a relationship between the age-related differences observed in visual white matter pathways and those observed in electrophysiology. Specifically, the maturation of the optic radiations during childhood fully mediates the changes observed in electrophysiological responses of the visual cortex.

These findings complement previous research linking diffusion and electrophysiological properties of the visual pathways in clinical and healthy adult populations (Alshowaeir et al. 2014; Berman et al. 2020; Kolbe et al. 2012; Lobsien et al.

2014; Naismith et al. 2010; M. Y. Takemura et al. 2017; H. Takemura, Yuasa, and Amano 2020). This study not only shows that there is a relationship between structural and functional properties of the visual system, but also that this relationship helps us better understand the development of response properties in the visual cortex during childhood. Between five and twelve years old the visual brain system undergoes a large range of transformations, allowing several visual skills to reach their full maturity (e.g., spatial acuity, contrast, and orientation sensitivity; Garey 1984; Siu and Murphy 2018). Part of these developmental differences are reflected by a greater structural integrity of the visual pathways (with a consequent increase of FA values) and by faster visually evoked responses (Armstrong, Slaven, and Harding 1991; Barnea-Goraly et al. 2005; Dayan et al. 2015; Onofrj et al. 2001). This study revealed that these two types of maturational variations are interrelated and, likely, that there is a directional connection that goes from structural to functional developmental changes. Future longitudinal work can establish the temporal sequence of structural and functional changes in the developing brain.

We could further characterize the link between brain structure and function by examining different visual tracts, stimuli, and tasks. The diffusion properties of the optic radiations and optic tracts were examined and a difference in their developmental trajectories emerged. Age-related differences in FA were evident for the optic radiations, but not for the optic tracts. This suggests that the structural properties of the

optic radiations continue maturing during late childhood (Dayan et al. 2015), while the optic tracts are largely stable within this age range. As a consequence, developmental differences in electrophysiology were mainly explained by the variation of optic radiations diffusion properties, and no additional variability was explained by the optic tracts. These findings suggest that not all the visual pathways account for visual signal delays over childhood, and that the optic radiation is the best candidate to account for electrophysiological variability in the visual cortex during this developmental window.

Moreover, by employing different visual stimuli and tasks we examined the extent to which structural-functional connection observed here could be generalized to distinct experimental conditions. Linear mixed effects models showed that children's M100 modulations depended on the optic radiations properties, and on the level of image contrast. Other experimental factors such as the level of noise of the image and the type of task performed did not have a significant impact on the M100, or on the M100-FA relationship. This suggests that the diffusion properties of the optic radiations predict a wide range of electrophysiological responses, which can be observed with different visual stimuli (readable and unreadable) and tasks (fixation and lexical decision tasks). Moreover, this structural-functional connection is particularly evident with larger and sharper M100 responses, such as those elicited by high contrast stimuli.

The present findings also allowed us to expand the functional significance of white matter diffusion properties by relating them to a number of electrophysiological

characteristics beyond latency (amplitude, power inter-trial coherence). Past studies have consistently proposed the latency of visually evoked responses as the most likely functional correlate of white matter structure (Alshowaeir et al. 2014; Berman et al. 2020; Dubois et al. 2008; Kolbe et al. 2012; Lobsien et al. 2014; Naismith et al. 2010; Price et al. 2017; M. Y. Takemura et al. 2017; H. Takemura, Yuasa, and Amano 2020). This choice is based on the assumption that the structural integrity of white matter tracts (and therefore, their related diffusion properties) has a great impact on the conduction velocity of neural signals (Alshowaeir et al. 2014; Berman et al. 2020; Kolbe et al. 2012; Lobsien et al. 2014; Naismith et al. 2010; M. Y. Takemura et al. 2017). However, apart from latency, we showed that time frequency estimates of visually evoked responses (power and inter-trial coherence) are also related to white matter diffusion properties. These electrophysiological measures present some advantages as compared to ERF measures (latency, amplitude). First, they usually show a reduced noise when single trials are analyzed within narrow frequency bands (Herrmann et al. 2014). Second, they better represent the degree of synchronization of oscillatory activity from large populations of neurons (even when it is not phase-locked to the stimulus onset, David, Kilner, and Friston 2006; Herrmann et al. 2014; Zhang 2019). These peculiarities of time frequency electrophysiological measures might facilitate the detection of correlations with diffusion properties and provide new insights on their functional interpretation. For example, future studies with larger samples could examine the coherence between

signals among multiple brain regions in relation to the tissue properties of the tracts that carry these signals. The presence of a relationship between diffusion and time frequency properties suggests that structural properties of white matter tracts can account, not only for the conduction velocity of neural signals, but also for additional aspects of the oscillatory neural activity such as its degree of synchronization.

In summary, these findings suggest that the maturation of visual white matter pathways over childhood accounts for variations in electrophysiological responses of the visual cortex. This structural-functional relationship is specific to the optic radiations and is stable across different tasks, levels of visual noise, and electrophysiological properties of the visual responses. The present findings are an example of how relating white matter properties to functional aspects of the brain can help us reach a more nuanced understanding of the link between development of brain connectivity and changes in electrophysiology.

References

Abdullah, Siti N., Nada Aldahlawi, Yanti Rosli, Vaegan, Mei Ying Boon, and Ted Maddess. 2012. "Effect of Contrast, Stimulus Density, and Viewing Distance on Multifocal Steady-State Visual Evoked Potentials (MSVs)." *Investigative Ophthalmology & Visual Science* 53 (9): 5527–35.

Allison, T., A. L. Hume, C. C. Wood, and W. R. Goff. 1984. "Developmental and Aging Changes in Somatosensory, Auditory and Visual Evoked Potentials." *Electroencephalography and Clinical Neurophysiology* 58 (1): 14–24.

Alshowaeir, Daniah, Con Yiannikas, Raymond Garrick, John Parratt, Michael H. Barnett, Stuart L. Graham, and Alexander Klistorner. 2014. "Latency of Multifocal Visual Evoked Potentials in Nonoptic Neuritis Eyes of Multiple Sclerosis Patients Associated with Optic Radiation Lesions." *Investigative Ophthalmology & Visual Science* 55 (6): 3758–64.

Andersson, Jesper L. R., Stefan Skare, and John Ashburner. 2003. "How to Correct Susceptibility Distortions in Spin-Echo Echo-Planar Images: Application to Diffusion Tensor Imaging." *NeuroImage* 20 (2): 870–88.

Andersson, Jesper L. R., and Stamatios N. Sotiropoulos. 2016. "An Integrated Approach to Correction for off-Resonance Effects and Subject Movement in Diffusion MR Imaging." *NeuroImage* 125 (January): 1063–78.

Armstrong, R. A., A. Slaven, and G. F. Harding. 1991. "Visual Evoked Magnetic Fields to Flash and Pattern in 100 Normal Subjects." *Vision Research* 31 (11): 1859–64.

Avants, B. B., C. L. Epstein, M. Grossman, and J. C. Gee. 2008. "Symmetric Diffeomorphic Image

Registration with Cross-Correlation: Evaluating Automated Labeling of Elderly and Neurodegenerative Brain." *Medical Image Analysis* 12 (1): 26–41.

Barnea-Goraly, Naama, Vinod Menon, Mark Eckert, Leanne Tamm, Roland Bammer, Asya Karchemskiy, Christopher C. Dant, and Allan L. Reiss. 2005. "White Matter Development during Childhood and Adolescence: A Cross-Sectional Diffusion Tensor Imaging Study." *Cerebral Cortex* 15 (12): 1848–54.

Berman, Shai, Yael Backner, Ronnie Krupnik, Friedemann Paul, Panayiota Petrou, Dimitrios Karussis, Netta Levin, and Aviv A. Mezer. 2020. "Conduction Delays in the Visual Pathways of Progressive Multiple Sclerosis Patients Covary with Brain Structure." *NeuroImage* 221 (November): 117204.

Cieslak, Matthew, Philip A. Cook, Xiaosong He, Fang-Cheng Yeh, Thijs Dhollander, Azeez Adebimpe, Geoffrey K. Aguirre, et al. 2020. "QSIPrep: An Integrative Platform for Preprocessing and Reconstructing Diffusion MRI." *Cold Spring Harbor Laboratory*. https://doi.org/10.1101/2020.09.04.282269.

Dale, A. M., B. Fischl, and M. I. Sereno. 1999. "Cortical Surface-Based Analysis. I. Segmentation and Surface Reconstruction." *NeuroImage* 9 (2): 179–94.

Dammers, Jurgen, Michael Schiek, Frank Boers, Carmen Silex, Mikhail Zvyagintsev, Uwe Pietrzyk, and Klaus Mathiak. 2008. "Integration of Amplitude and Phase Statistics for Complete Artifact Removal in Independent Components of Neuromagnetic Recordings." *IEEE Transactions on Biomedical Engineering*. https://doi.org/10.1109/tbme.2008.926677.

David, Olivier, James M. Kilner, and Karl J. Friston. 2006. "Mechanisms of Evoked and Induced Responses in MEG/EEG." *NeuroImage* 31 (4): 1580–91.

Dayan, Michael, Monica Munoz, Sebastian Jentschke, Martin J. Chadwick, Janine M. Cooper, Kate Riney, Faraneh Vargha-Khadem, and Chris A. Clark. 2015. "Optic Radiation Structure and Anatomy in the Normally Developing Brain Determined Using Diffusion MRI and Tractography." *Brain Structure & Function* 220 (1): 291–306.

Dhollander, Thijs, David Raffelt, and Alan Connelly. 2016. "Unsupervised 3-Tissue Response Function Estimation from Single-Shell or Multi-Shell Diffusion MR Data without a Co-Registered T1 Image." In *ISMRM Workshop on Breaking the Barriers of Diffusion MRI*, 5:5.

Dhollander, T., R. Mito, D. Raffelt, and A. Connelly. 2019. "Improved White Matter Response Function Estimation for 3-Tissue Constrained Spherical Deconvolution." In *Proc. Intl. Soc. Mag. Reson. Med*. Vol. 555.

Dubois, Jessica, Ghislaine Dehaene-Lambertz, Catherine Soarès, Yann Cointepas, Denis Le Bihan, and Lucie Hertz-Pannier. 2008. "Microstructural Correlates of Infant Functional Development: Example of the Visual Pathways." *The Journal of Neuroscience: The Official Journal of the Society for Neuroscience* 28 (8): 1943–48.

Fan, Lingzhong, Hai Li, Junjie Zhuo, Yu Zhang, Jiaojian Wang, Liangfu Chen, Zhengyi Yang, et al. 2016. "The Human Brainnetome Atlas: A New Brain Atlas Based on Connectional Architecture." *Cerebral Cortex* 26 (8): 3508–26.

Fischl, B., M. I. Sereno, R. B. Tootell, and A. M. Dale. 1999. "High-Resolution Intersubject Averaging and a Coordinate System for the Cortical Surface." *Human Brain Mapping* 8 (4): 272–84.

Fonov, V. S., A. C. Evans, R. C. McKinstry, C. R. Almli, and D. L. Collins. 2009. "Unbiased Nonlinear Average Age-Appropriate Brain Templates from Birth to Adulthood."

NeuroImage Supplement 1 (47): S102.

Garey, L. J. 1984. "Structural Development of the Visual System of Man." *Human Neurobiology* 3 (2): 75–80.

Gebodh, Nigel, M. Isabel Vanegas, and Simon P. Kelly. 2017. "Effects of Stimulus Size and Contrast on the Initial Primary Visual Cortical Response in Humans." *Brain Topography* 30 (4): 450–60.

Gilmore, John H., Rebecca C. Knickmeyer, and Wei Gao. 2018. "Imaging Structural and Functional Brain Development in Early Childhood." *Nature Reviews. Neuroscience* 19 (3): 123–37.

Gorgolewski, K. J., O. Esteban, C. J. Markiewicz, E. Ziegler, D. G. Ellis, M. P. Notter, D. Jarecka, et al. 2018. "Nipype." *Software: Practice & Experience*.

Gorgolewski, Krzysztof, Christopher D. Burns, Cindee Madison, Dav Clark, Yaroslav O. Halchenko, Michael L. Waskom, and Satrajit S. Ghosh. 2011. "Nipype: A Flexible, Lightweight and Extensible Neuroimaging Data Processing Framework in Python." *Frontiers in Neuroinformatics*. https://doi.org/10.3389/fninf.2011.00013.

Gramfort, Alexandre, Martin Luessi, Eric Larson, Denis A. Engemann, Daniel Strohmeier, Christian Brodbeck, Roman Goj, et al. 2013. "MEG and EEG Data Analysis with MNE-Python." *Frontiers in Neuroscience* 7 (December): 267.

Hämäläinen, M. S., and R. J. Ilmoniemi. 1994. "Interpreting Magnetic Fields of the Brain: Minimum Norm Estimates." *Medical & Biological Engineering & Computing* 32 (1): 35–42.

Hämäläinen, M. S., and J. Sarvas. 1989. "Realistic Conductivity Geometry Model of the Human Head for Interpretation of Neuromagnetic Data." *IEEE Transactions on Bio-Medical*

Engineering 36 (2): 165–71.

Herrmann, Christoph S., Stefan Rach, Johannes Vosskuhl, and Daniel Strüber. 2014. "Time-Frequency Analysis of Event-Related Potentials: A Brief Tutorial." *Brain Topography* 27 (4): 438–50.

Hulley, Stephen B., Steven R. Cummings, Warren S. Browner, Norman Hearst, Deborah Grady, Thomas B. Newman, and Thomas B. Newman. 2001. *Designing Clinical Research: An Epidemiologic Approach*. Lippincott Williams & Wilkins.

Jeurissen, Ben, Maxime Descoteaux, Susumu Mori, and Alexander Leemans. 2019. "Diffusion MRI Fiber Tractography of the Brain." *NMR in Biomedicine* 32 (4): e3785.

Joliot, Marc, Gaël Jobard, Mikaël Naveau, Nicolas Delcroix, Laurent Petit, Laure Zago, Fabrice Crivello, Emmanuel Mellet, Bernard Mazoyer, and Nathalie Tzourio-Mazoyer. 2015. "AICHA: An Atlas of Intrinsic Connectivity of Homotopic Areas." *Journal of Neuroscience Methods* 254 (October): 46–59.

Joo, Sung Jun, Kambiz Tavabi, Sendy Caffarra, and Jason D. Yeatman. 2021. "Automaticity in the Reading Circuitry." *Brain and Language* 214 (March): 104906.

Kanai, Ryota, and Geraint Rees. 2011. "The Structural Basis of Inter-Individual Differences in Human Behaviour and Cognition." *Nature Reviews. Neuroscience* 12 (4): 231–42.

Kiesel, Andrea, Jeff Miller, Pierre Jolicœur, and Benoit Brisson. 2008. "Measurement of ERP Latency Differences: A Comparison of Single-Participant and Jackknife-Based Scoring Methods." *Psychophysiology*. https://doi.org/10.1111/j.1469-8986.2007.00618.x.

Kolbe, Scott, Clare Bajraszewski, Caron Chapman, Tan Nguyen, Peter Mitchell, Mark Paine, Helmut Butzkueven, Leigh Johnston, Trevor Kilpatrick, and Gary Egan. 2012. "Diffusion

Tensor Imaging of the Optic Radiations after Optic Neuritis." *Human Brain Mapping* 33 (9): 2047–61.

Kolb, Helga, Eduardo Fernandez, and Ralph Nelson. 2005. "The Organization of the Retina and Visual System." *Webvision-The Organization of the Retina and Visual System*. https://europepmc.org/books/n/webvision/?extid=21413386&src=med.

Kruper, John, Jason D. Yeatman, Adam Richie-Halford, David Bloom, Mareike Grotheer, Sendy Caffarra, Gregory Kiar, Iliana I. Karipidis, Ethan Roy, and Ariel Rokem. 2021. "Evaluating the Reliability of Human Brain White Matter Tractometry." *bioRxiv*. https://doi.org/10.1101/2021.02.24.432740.

Lebel, C., M. Gee, R. Camicioli, M. Wieler, W. Martin, and C. Beaulieu. 2012. "Diffusion Tensor Imaging of White Matter Tract Evolution over the Lifespan." *NeuroImage* 60 (1): 340–52.

Lebel, C., L. Walker, A. Leemans, L. Phillips, and C. Beaulieu. 2008. "Microstructural Maturation of the Human Brain from Childhood to Adulthood." *NeuroImage* 40 (3): 1044–55.

Lobsien, D., B. Ettrich, K. Sotiriou, J. Classen, F. Then Bergh, and K-T Hoffmann. 2014. "Whole-Brain Diffusion Tensor Imaging in Correlation to Visual-Evoked Potentials in Multiple Sclerosis: A Tract-Based Spatial Statistics Analysis." *AJNR. American Journal of Neuroradiology* 35 (11): 2076–81.

Maddess, Ted, Andrew Charles James, and Elizabeth Anne Bowman. 2005. "Contrast Response of Temporally Sparse Dichoptic Multifocal Visual Evoked Potentials." *Visual Neuroscience* 22 (2): 153–62.

Maris, Eric, and Robert Oostenveld. 2007. "Nonparametric Statistical Testing of EEG- and MEG-

Data." *Journal of Neuroscience Methods* 164 (1): 177–90.

Mosher, John C., Richard M. Leahy, David W. Shattuck, and Sylvain Baillet. 1999. "MEG Source Imaging Using Multipolar Expansions." In *Information Processing in Medical Imaging*, 15–28. Springer Berlin Heidelberg.

Naismith, R. T., J. Xu, N. T. Tutlam, K. Trinkaus, A. H. Cross, and S-K Song. 2010. "Radial Diffusivity in Remote Optic Neuritis Discriminates Visual Outcomes." *Neurology* 74 (21): 1702–10.

Odom, J. Vernon, Michael Bach, Colin Barber, Mitchell Brigell, Michael F. Marmor, Alma Patrizia Tormene, Graham E. Holder, and Vaegan. 2004. "Visual Evoked Potentials Standard (2004)." *Documenta Ophthalmologica. Advances in Ophthalmology* 108 (2): 115–23.

Onofrj, M., A. Thomas, D. Iacono, G. D'Andreamatteo, and C. Paci. 2001. "Age-Related Changes of Evoked Potentials." *Neurophysiologie Clinique/Clinical Neurophysiology*. https://doi.org/10.1016/s0987-7053(01)00248-9.

Price, D., Cam-CAN, L. K. Tyler, R. Neto Henriques, K. L. Campbell, N. Williams, M. S. Treder, J. R. Taylor, and R. N. A. Henson. 2017. "Age-Related Delay in Visual and Auditory Evoked Responses Is Mediated by White- and Grey-Matter Differences." *Nature Communications*. https://doi.org/10.1038/ncomms15671.

Raffelt, David, Thijs Dhollander, J-Donald Tournier, Rami Tabbara, Robert E. Smith, Eric Pierre, and Alan Connelly. 2017. "Bias Field Correction and Intensity Normalisation for Quantitative Analysis of Apparent Fibre Density." In *Proc. Intl. Soc. Mag. Reson. Med*, 25:3541.

Sherbondy, Anthony J., Robert F. Dougherty, Sandy Napel, and Brian A. Wandell. 2008.

"Identifying the Human Optic Radiation Using Diffusion Imaging and Fiber Tractography." *Journal of Vision* 8 (10): 12.1–11.

Siu, Caitlin R., and Kathryn M. Murphy. 2018. "The Development of Human Visual Cortex and Clinical Implications." *Eye and Brain* 10 (April): 25–36.

Smith, Stephen M., Mark Jenkinson, Mark W. Woolrich, Christian F. Beckmann, Timothy E. J. Behrens, Heidi Johansen-Berg, Peter R. Bannister, et al. 2004. "Advances in Functional and Structural MR Image Analysis and Implementation as FSL." *NeuroImage* 23 Suppl 1: S208–19.

Spear, P. D. 1993. "Neural Bases of Visual Deficits during Aging." *Vision Research* 33 (18): 2589–2609.

Takemura, Hiromasa, Kenichi Yuasa, and Kaoru Amano. 2020. "Predicting Neural Response Latency of the Human Early Visual Cortex from MRI-Based Tissue Measurements of the Optic Radiation." *eNeuro* 7 (4). https://doi.org/10.1523/ENEURO.0545-19.2020.

Takemura, Mariko Yoshida, Masaaki Hori, Kazumasa Yokoyama, Nozomi Hamasaki, Michimasa Suzuki, Koji Kamagata, Kouhei Kamiya, et al. 2017. "Alterations of the Optic Pathway between Unilateral and Bilateral Optic Nerve Damage in Multiple Sclerosis as Revealed by the Combined Use of Advanced Diffusion Kurtosis Imaging and Visual Evoked Potentials." *Magnetic Resonance Imaging* 39 (June): 24–30.

Taulu, Samu, and Riitta Hari. 2009. "Removal of Magnetoencephalographic Artifacts with Temporal Signal-Space Separation: Demonstration with Single-Trial Auditory-Evoked Responses." *Human Brain Mapping* 30 (5): 1524–34.

Taulu, Samu, and Matti Kajola. 2005. "Presentation of Electromagnetic Multichannel Data: The

Signal Space Separation Method." *Journal of Applied Physics* 97 (12): 124905.

Tingley, Dustin, Teppei Yamamoto, Kentaro Hirose, Luke Keele, and Kosuke Imai. 2014. "Mediation:RPackage for Causal Mediation Analysis." *Journal of Statistical Software* 59 (5): 1–38.

Tournier, J-Donald, Fernando Calamante, David G. Gadian, and Alan Connelly. 2004. "Direct Estimation of the Fiber Orientation Density Function from Diffusion-Weighted MRI Data Using Spherical Deconvolution." *NeuroImage* 23 (3): 1176–85.

Tournier, J-Donald, Robert Smith, David Raffelt, Rami Tabbara, Thijs Dhollander, Maximilian Pietsch, Daan Christiaens, Ben Jeurissen, Chun-Hung Yeh, and Alan Connelly. 2019. "MRtrix3: A Fast, Flexible and Open Software Framework for Medical Image Processing and Visualisation." *NeuroImage* 202 (November): 116137.

Tournier, J-Donald, Chun-Hung Yeh, Fernando Calamante, Kuan-Hung Cho, Alan Connelly, and Ching-Po Lin. 2008. "Resolving Crossing Fibres Using Constrained Spherical Deconvolution: Validation Using Diffusion-Weighted Imaging Phantom Data." *NeuroImage* 42 (2): 617–25.

Tustison, Nicholas J., Brian B. Avants, Philip A. Cook, Yuanjie Zheng, Alexander Egan, Paul A. Yushkevich, and James C. Gee. 2010. "N4ITK: Improved N3 Bias Correction." *IEEE Transactions on Medical Imaging* 29 (6): 1310–20.

Vialatte, François-Benoît, Monique Maurice, Justin Dauwels, and Andrzej Cichocki. 2010. "Steady-State Visually Evoked Potentials: Focus on Essential Paradigms and Future Perspectives." *Progress in Neurobiology* 90 (4): 418–38.

Wandell, Brian A. 2016. "Clarifying Human White Matter." *Annual Review of Neuroscience*.

https://doi.org/10.1146/annurev-neuro-070815-013815.

Yeatman, Jason D., Robert F. Dougherty, Nathaniel J. Myall, Brian A. Wandell, and Heidi M. Feldman. 2012. "Tract Profiles of White Matter Properties: Automating Fiber-Tract Quantification." *PloS One* 7 (11): e49790.

Yeatman, Jason D., Brian A. Wandell, and Aviv A. Mezer. 2014. "Lifespan Maturation and Degeneration of Human Brain White Matter." *Nature Communications* 5 (September): 4932.

Zhang, Y., M. Brady, and S. Smith. 2001. "Segmentation of Brain MR Images through a Hidden Markov Random Field Model and the Expectation-Maximization Algorithm." *IEEE Transactions on Medical Imaging* 20 (1): 45–57.

Zhang, Zhiguo. 2019. "Spectral and Time-Frequency Analysis." In *EEG Signal Processing and Feature Extraction*, edited by Li Hu and Zhiguo Zhang, 89–116. Singapore: Springer Singapore.

Supplementary Materials

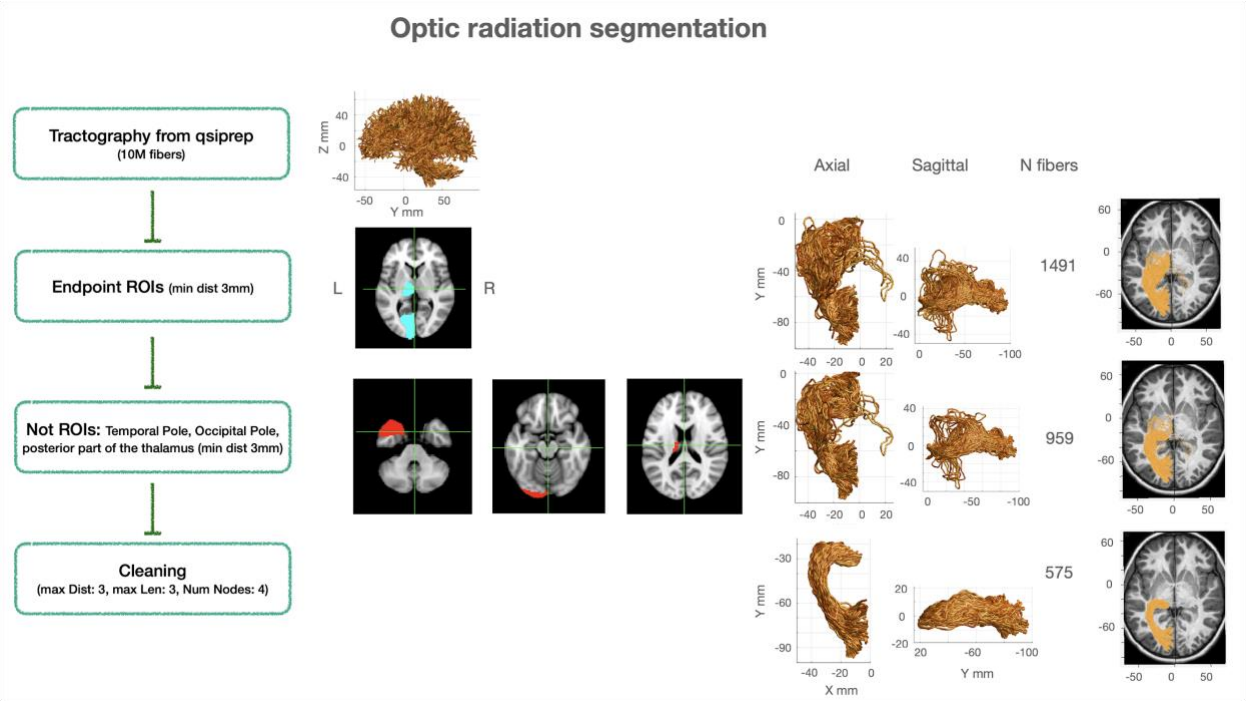

Figure S1. Schematic representation of the optic radiations segmentation. On the left side, each step of the pipeline is described. The middle column shows the tractography reconstructed from qsiprep, and the ROIs used to track the bundle. On the right side, the same optic radiation of an example participant is plotted for each step of analysis.

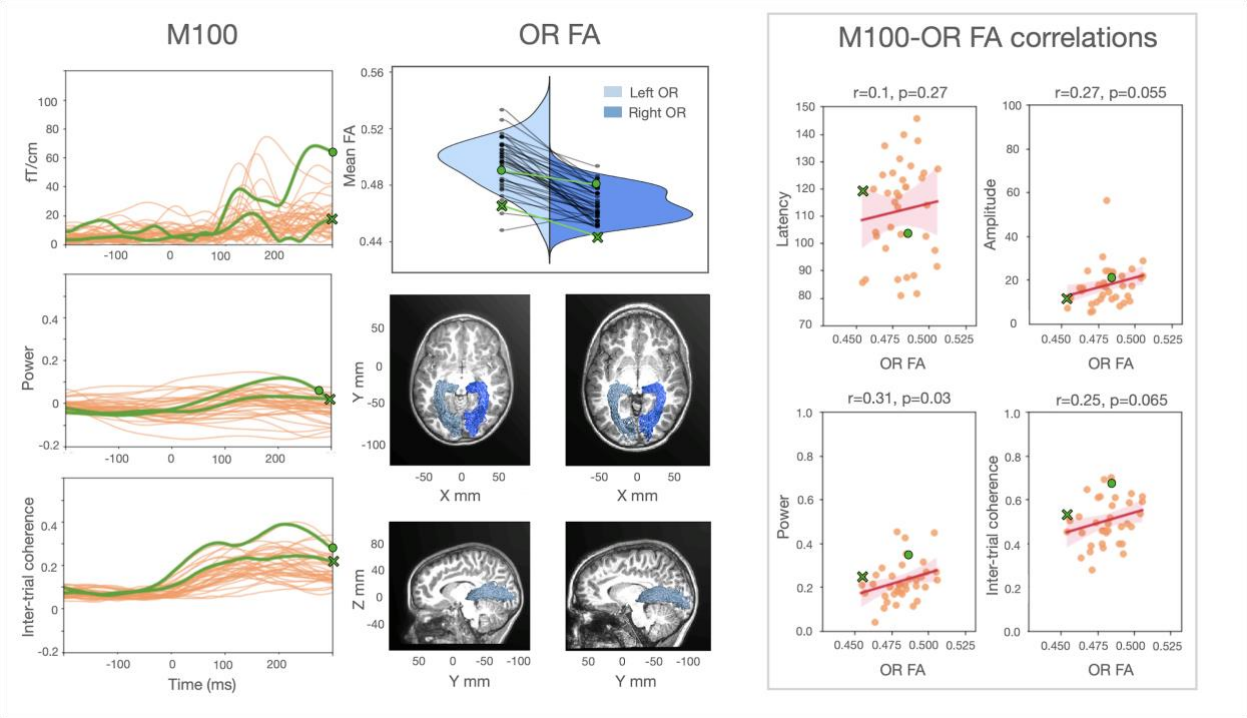

Figure S2. The relation between structural and functional properties of the visual pathways in the low contrast condition. **M100 panel:** Individual ERFs, power and inter-trial coherence average values (between 1 and 8 Hz) are displayed over time. The occipital responses of the same two representative subjects shown in Figure 3 are highlighted (green dot for the faster response and green cross for the slower one). **OR FA panel:** Violin plot of the individual FA values from the left and right optic radiations. Sagittal and axial views of the optic radiations for the two representative participants are overlaid on each subject's structural image. **M100-OR FA correlations panel:** Correlations between MEG measures and optic radiations FA mean values (robust correlations for latency: r=+0.09, p=0.30; amplitude: r=+0.37, p=0.01; power: r=+0.31, p=0.03; inter-trial coherence: r=+0.26, p=0.06). A full FA mediation effect was visible only for the M100 amplitude (average causal mediation effect: β=4.8e-15, *CI* [+1.3e-16; +1.2e-14], p=0.04; average direct effect: β=-1.0e-14, *CI* [-3.1e-14; +5.7e-15], p=0.26)